Molecular dynamics simulations of a new branched antimicrobial peptide: A comparison of force fields

Jianguo Li, Rajamani Lakshminarayanan, Yang Bai, Shouping Liu, Lei Zhou, Konstantin Pervushin, Chandra Verma, and Roger W. Beuerman

Citation: The Journal of Chemical Physics **137**, 215101 (2012); doi: 10.1063/1.4768899
View online: http://dx.doi.org/10.1063/1.4768899
View Table of Contents: http://scitation.aip.org/content/aip/journal/jcp/137/21?ver=pdfcov
Published by the AIP Publishing

Molecular dynamics simulations of a new branched antimicrobial peptide: A comparison of force fields

Jianguo Li,[1,2,a)] Rajamani Lakshminarayanan,[1] Yang Bai,[1,3] Shouping Liu,[1,3] Lei Zhou,[1] Konstantin Pervushin,[3] Chandra Verma,[1,2,3,4,a)] and Roger W. Beuerman[1,2,5]
[1]*Singapore Eye Research Institute, 11 Third Hospital Avenue, #06-00, Singapore 168751*
[2]*Bioinformatics Institute (A-STAR), 30 Biopolis Street, #07-01 Matrix, Singapore 138671*
[3]*School of Biological Sciences, Nanyang Technological University, Singapore 637551*
[4]*Department of Biological Sciences, National University of Singapore, Singapore 117543*
[5]*Duke-NUS, SRP Neuroscience-Behaviroal Disorders, Singapore*

(Received 29 August 2012; accepted 12 November 2012; published online 4 December 2012)

Branched antimicrobial peptides are promising as a new class of antibiotics displaying high activity and low toxicity and appear to work through a unique mechanism of action. We explore the structural dynamics of a covalently branched 18 amino acid peptide (referred to as B2088) in aqueous and membrane mimicking environments through molecular dynamics (MD) simulations. Towards this, we carry out conventional MD simulations and supplement these with replica exchange simulations. The simulations are carried out using four different force fields that are commonly employed for simulating biomolecular systems. These force fields are GROMOS53a6, CHARMM27 with cMAP, CHARMM27 without cMAP and AMBER99sb. The force fields are benchmarked against experimental data available from circular dichroism and nuclear magnetic resonance spectroscopies, and show that CHARMM27 without cMAP correction is the most successful in reproducing the structural dynamics of B2088 both in water and in the presence of micelles. Although the four force fields predict different structures of B2088, they all show that B2088 stabilizes against the head group of the lipid through hydrogen bonding of its Lys and Arg side chains. This leads us to hypothesize that B2088 is unlikely to penetrate into the hydrophobic region of the membrane owing to the high free energy costs of transfer from water, and possibly acts by carpeting and thus disrupting the membrane.
 [http://dx.doi.org/10.1063/1.4768899]

I. INTRODUCTION

Antimicrobial peptides (AMPs), generally less than 40 amino acids in length, are being investigated in the search for new antibiotics as the traditional ones are increasingly being rendered ineffective with the rise of resistant bacteria.[1–5] Unlike traditional antibiotics, it is thought that AMPs do not lead to bacterial resistance because they primarily target, non-specifically, bacterial membranes rather than specific bacterial proteins.[1,3] Although there are more than 1700 naturally occurring or artificially designed AMPs, their lengths and sequences differ significantly, thus making it difficult to relate the sequence to activity. Nevertheless, they share common features including high cationicity and richness in hydrophobic residues, forming amphiphilic molecules.

Recently, we have designed a new class of branched AMPs by crosslinking the two C-terminal segments of human β-defensin3 through the α- and ε-amino groups of lysine.[6–8] These branched peptides have demonstrated significantly higher antimicrobial activity and lower toxicity than the monomer or native human defensins. The main structural feature of these peptides that somehow endows the peptide with enhanced activity appears to be the existence of the branched topology in which two peptide chains are covalently linked. The minimum inhibitory concentration of a branched AMP that we refer to as B2088 is 20 times lower than that of the corresponding unbranched analogue, the V2-monomer.[7] In addition, the branched AMPs carry a high percentage of positively charged Lys and Arg residues (+12 charge over 18 residues), which steer the peptide towards the negatively charged bacterial membrane.[9,10] In this study, we combine molecular dynamics (MD) simulations with data obtained from nuclear magnetic resonance (NMR) and circular dichroism (CD) experiments to probe the structure and dynamics of the newly developed branched peptide B2088, both in aqueous solution and in the presence of micelles. Figure 1 shows the chemical structure of B2088. The peptide has two chains covalently linked through the ε-amino group of Lys9. Both the primary chain (RGRKVVRRKK) and the secondary chain (RGRKVVRR) are the analogs of the C-terminus of human defensin[11] (pdb id: 1KJ6). The secondary chain is linked to the primary chain through the side chain $-NH_3$ of Lys9, thus forming a branched structure. Initially, it would be expected that the electrostatic repulsion among the positive charges would favor an extended structure. On the other hand, the branched core brings the two strands close and favors a compact structure stabilized by hydrophobic interactions. Thus, how the competition of the two factors (i.e., high charge and branched core) affect the folding of B2088 is of great interest, not only because of its clinical application as a scaffold for potential antimicrobial drugs but also because it can reveal the physics governing the folding of branched

a)Authors to whom correspondence should be addressed. Electronic addresses: lijg@bii.a-star.edu.sg and chandra@bii.a-star.edu.sg.

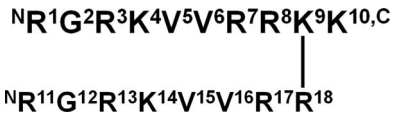

FIG. 1. Chemical structure of B2088.

peptides and assist in the design of analogues with improved properties.

Atomistic and coarse-grained MD simulations have been used extensively to study the folding of both small peptides and proteins. However, a major unresolved issue in MD simulations is the choice of the appropriate force field. For biomolecules, currently there are four popular categories of force fields: GROMOS,[12] CHARMM,[13] AMBER,[14] and OPLS,[15] and each category includes several versions. For example, the family of AMBER force fields consists of versions AMBER94, AMBER99sb,[16] AMBERGS,[17] AMBER03,[18] etc. Several studies using these force fields suggest that these force fields properly balance the bonded and non-bonded contributions and are reliable in most cases.[19] Nevertheless, due to the empirical (or semi-empirical) parameters of each force field, the parameterization procedure of each force field varies. The difference in the force field parameters, together with different water models for each force field, may lead to significantly different results.[20–25] This suggests that for any system that is being simulated, an appropriate choice of the force field needs to be made. In particular, since we are examining a new molecule, it is necessary to establish the force field most suited to capture the experimental structural and dynamical properties.

Most studies investigating the accuracies of force fields have examined their ability to reproduce the widely available experimental data on the conformational landscape of model short polyalanine peptides $(Ala)_n$.[26–30] For example, replica exchange molecular dynamics (REMD) simulations of the folding of polyalanine showed that most current force fields have a bias for stabilizing the helical structure.[30] NMR and REMD studies of penta-alanine peptide[26] revealed that AMBER03 and OPLS/AA produce structures in excellent agreement with experimental results, but AMBERGS and GROMOS53a6 lead to marked deviations from experimental results. Yoda *et al.*[22,31] found that AMBER99 and CHARMM22 are suitable for helical peptides, while OPLS-AA/L and GROMOS96 are appropriate for peptides with a β-sheet structure. Lange *et al.*[24] showed that the accuracy of the simulation results not only depends on the force field parameters, but also on the treatment of electrostatic interactions. The authors found that the particle-mesh Ewald (PME) method yields results that are more accurate than cutoff and reaction-field methods and that the AMBER99sb force field produces data that are most consistent with NMR. Besides the force field, MD simulations of protein folding also suffer from the sampling problem. During simulations, peptides/proteins are frequently trapped in local minima of free energy surfaces, which have very complex topologies. To overcome these difficulties, biased simulation algorithms such as REMD simulations and umbrella sampling have been developed. As a hybrid method combining both MD and Monte Carlo (MC) algorithms, REMD simulations have been shown to accurately capture not only the thermodynamics, but also the dynamics of protein folding.[32,33]

In this study, we explore the conformations of B2088 by applying REMD simulations in aqueous environment and conventional MD simulations in lipid environment using four different force fields: GROMOS53a6,[34] AMBER99sb,[16] CHARMM27 with cMAP correction,[13] and CHARMM27 without cMAP correction[35] (we will refer to the latter two force fields as cMAP CHARMM and CHARMM, respectively). The reasons we choose these four force fields are (i) GROMOS and CHARMM force fields have been found to be relatively accurate for both protein and lipids and have been used for most membrane simulations; (ii) AMBER99sb has repeatedly been shown to be very good for protein simulations[24,36–38] and is compatible with the general AMBER force field which is developed for simulating organic molecules including lipids.[39,40] Further, to understand the action of B2088, we need to understand its interactions with bacterial membranes in detail. Towards this, using the four force fields, we first constructed a model anionic micelle that mimics the bacterial membrane, and then investigated the interaction of B2088 with the anionic micelle. These were then compared with data available from CD and NMR experiments. The results presented in this study not only enhance our understanding of the folding mechanism of the branched peptide B2088, but also reveal possible modes of interactions of B2088 with lipids and help hypothesize its mode of action.

II. METHODS

A. Model peptide

The structure of the model branched peptide B2088 $(RGRKVVRR)_2KK$ is shown in Figure 1. It has two positively charged N-termini and one negatively charged C-terminus. The initial structure of B2088 was constructed using Discovery Studio 2.5 (Accelrys, San Diego, CA). The protonation state of the charged residues was determined at pH 7, resulting in 12 positive charges. The atom types as well as the charge on the nitrogen atom in the side chain of Lys at the branch site are set to be the same as that on the nitrogen of the amide backbone. Temperature REMD simulations of B2088 in water and conventional MD simulations of B2088 with micelles were carried out using the GROMACS package since the recently released GROMACS-4.5 allows us to use all the above mentioned force fields and thus avoid any bias resulting from using different simulation packages.[41]

B. REMD simulations

REMD simulations were performed to investigate the solution structure of B2088. The peptide was modeled using four force fields: GROMOS53a6, AMBER99sb, cMAP CHARMM, and CHARMM. The TIP3P water model[42] was used during all the simulations except for the GROMOS53a6 force field, in which the SPC water model was used.[43] A random conformation of the peptide was chosen and was immersed in a cubic box of 5.5 nm in length with about 5000

water molecules. Twelve counterions were added to neutralize the system. Then the system was subjected to 500 steps of energy minimization using the steepest descent algorithm followed by MD simulations for 20 ns at 400 K. This gave rise to a random peptide structure that was used as the starting conformation for the subsequent REMD simulations. In each REMD simulation, 26 replicas with temperature exponentially spaced between 298 K and 400.2 K were generated online based on the work of Patriksson and van der Spoel.[44] As B2088 only has 18 residues, the highest temperature used in the REMD simulations (400.2 K) is assumed to be sufficient to bring the peptide out of local minima (see the supplementary material Figure S1).[45] For every 0.5 ps, one MC move between adjacent temperatures is performed. An acceptance ratio of 0.1 was achieved to ensure a sufficient exchange rate. Each REMD simulation was performed for 200 ns, which corresponds to a total simulation time of 20.8 μs for the four force fields. The secondary structure evolution of B2088 during the REMD simulations was calculated using DSSP.[46] In all simulations, the MD time step is 2 fs. A cutoff distance of 1.2 nm was used for both the Lennard-Jones (LJ) and real-space electrostatic interactions, and the particle-mesh Ewald algorithm was employed to calculate the long-range electrostatic interactions in reciprocal space. The Berendsen coupling method[47] was used to maintain the target temperatures in REMD simulations and the pressure was maintained at 1 atm in the *NPT* ensemble.

C. MD simulations in the presence of micelles

Conventional MD simulations were carried out to examine the interaction of B2088 with lipids. We used an anionic micelle consisting of dodecylphosphocholine (DPC) and 1-palmitoyl-2-oleoyl-sn-glycero-3-phosphoglycerol (POPG) with a DPC:POPG ratio of 3:1 to mimic a bacterial membrane. We did not use temperature REMD for peptide-micelle simulations because the micelle will be unstable at high temperatures. For the peptide, the same four force fields were employed for the simulations: GROMOS53a6, AMBER99sb, cMAP CHARMM, and CHARMM. In the case of the GROMOS53a6 force field, the Berger parameters were used for the lipids,[48] while for CHARMM, the recently developed CHARMM36 parameters were used.[49] In the case of the AMBER99sb force field, the lipid parameters were obtained using the Antechamber utility in the AMBER 10 package.[50,51] We used micelles consisting of 64 lipids, with 48 zwitterionic DPC and 16 anionic POPG to mimic the bacterial membrane. In order to generate an appropriate starting model of the micelle, 16 POPG and 48 DPC lipids were randomly placed in the simulation box with water and counterions added. The system was subjected to simulations for 100 ns during which we noticed that lipids quickly self-assembled into micelles (e.g., within 60 ns) and remained stable during the remainder of the simulations, as shown in the supplementary material Figure S2.[45] The coordinates at the end of 100 ns were then taken, and the branched peptide B2088 with a random structure placed 2.5 nm away from the micelle surface in a cubic simulation box of 9 nm. The simulation box was further solvated with roughly 22 000 water molecules and 4 Na+ ions. For each force field, a 400 ns MD simulation at 298 K was performed; the simulation details are the same as those for the REMD simulations.

D. CD spectropolarimetry and NMR experiments

A JASCO J-810 circular dichroism spectropolarimeter was used to perform the CD experiments. The branched peptide B2088 (0.25 mg/ml) was dissolved in water, or in water with vesicles. The far UV-CD spectra was recorded using a 0.1-cm path length quartz cuvette under constant nitrogen flush at a scan rate of 50 nm/min, with a step size of 0.1 nm, bandwidth of 2 nm, and an averaging time of 3 s. The final spectra reported were an average of 4 scans and had the background data removed. The small unilamellar vesicles were prepared from a mixture of POPC (1-palmitoyl-2-oleoyl-sn-glycero-3-phosphocholine) and POPG at 7:3 (w/w). The lipid mixture was dissolved in chloroform, dried under a stream of nitrogen, and lyophilized overnight. The lipid film was rehydrated with 20 mM phosphate buffer (pH 7.0), sonicated for 30 min, freeze-thawed for 10 cycles, and sonicated for an additional 1 h. An aliquot of B2088 was added to the lipid suspension to give a peptide:lipid molar ratio of 1:7 and CD spectra was recorded as before.

NMR experiments were performed using Bruker Avance II 700 MHz spectrometer at 25 °C for aqueous and micelle solutions in a cryo-probe. Lipid micelles were prepared by dissolving 5.3 mg DPC and 5.0 mg POPG (from Avanti Polar Lipids) in 0.5 ml of phosphate buffer (30 mM). The final 500 μl NMR sample contained 1 mM labeled B2088 peptide in DPC-POPG mixed micelles (DPC 30 mM, POPG 13 mM). Two-dimensional homo-nuclear TOCSY, NOESY, and ROESY experiments were conducted with mixing times of 70, 200, and 100 ms, respectively. Hetero-nuclear ^{1}H-^{13}C (^{15}N) HSQC, HNCA, ^{15}N-NOESY spectra were acquired. Residue specific resonance assignments and assignments of NOESY cross-peaks were performed using CARA (www.nmr.ch). 3D structures of the B2088 peptide in DPC-POPG mixed micelles were reconstructed using CYANA 3.0.[52] Comparison of the simulated and experimental structures was carried out by aligning the backbone atomic coordinates of the most probable structures predicted by each force field on to a structure determined using NMR.[7]

III. RESULTS AND DISCUSSION

We first examine how the REMD simulations describe folding of B2088 in solution using the four force fields. Next, we examine the force field dependence of the interactions of B2088 with anionic micelles that mimic the bacterial membrane. The simulations are compared with parameters derived from CD and NMR experiments (e.g., radius of gyration (Rg), surface area (Sa), structural alignment) to examine the accuracy of each force field. Finally, the mode of interaction of B2088 with micelles and implications for the mechanism of action of B2088 are discussed.

A. Solution structure of the branched peptide B2088

As mentioned above, the peptide must be characterized by a frustrated energy landscape where a conflict exists

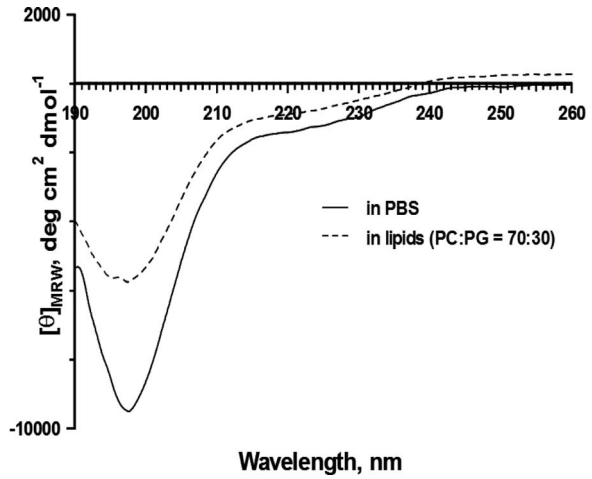

FIG. 2. Circular dichroism spectroscopy of B2088 in water and lipid environments.

between electrostatic repulsion (between the charged side chains that will result in the two peptide chains remaining extended) and the cross-link that will attempt to bring the two peptide chains together. The CD spectra (Figure 2) of B2088 in water displayed a strong minimum around 197 nm, a signature of a coiled structure in water. This lack of any residual structure in water has earlier been reported by NMR experiments.[7] However, from the simulations it is clear that the four force fields give rise to significantly different secondary structures of B2088 (Figure 3). GROMOS53a6 yields stable β-sheet structures while cMAP CHARMM favors α-helical structures. The other two force fields, CHAMRM and AMBER99sb, give rise to coiled conformations that are consistent with both CD and NMR. In the case of GROMOS53a6, the folding is fast, indicating a strong propensity to form a β-sheet structure. After 100 ns, a stable anti-parallel β-sheet structure is formed between the two KVVRR segments of the two branches. Note that the two segments (KVVRR) are covalently connected at Lys9 of the primary chain. Therefore, the existence of the branched site seems to favor the formation of β-sheet structure. In addition, the hydrophobic association of the four Val residues further stabilizes the β-sheet conformation. This tendency of GROMOS53a6 to overestimate the β-sheet structure is consistent with previous studies.[22,23,31] In contrast, cMAP CHARMM overestimates the α-helical structure, which mostly disappears when the cMAP correction is removed (leading instead to some instantaneous π-helical conformations), as can be seen in Figure 3(c). This seems reasonable since cMAP was initially designed to reproduce the α-helical structures of the polyalanine peptide by applying corrections to the backbone dihedral potentials,[13,53] and it has been shown in some simulations that without the cMAP correction, the CHARMM force field generates π-helical polyalanine.[54] While the conformation of the polyalanine peptide is largely determined by the backbone dihedral potentials due to the small side chain of alanine, the conformation of B2088 will be affected by both backbone dihedral and side chain interactions. It is clear that the introduction of the cMAP correction for the backbone dihedrals appears to bias the balance between the side chain interactions and backbone dihedral potentials of B2088, resulting in overestimation of α-helical structure of B2088. Indeed, similar observations have been made for other non-polyalanine peptides,[55,56] such as the human Pin1 WW domain where the removal of the cMAP correction changed the free energy surface from favoring the α-helical structure to one favoring the native β-sheet.[55]

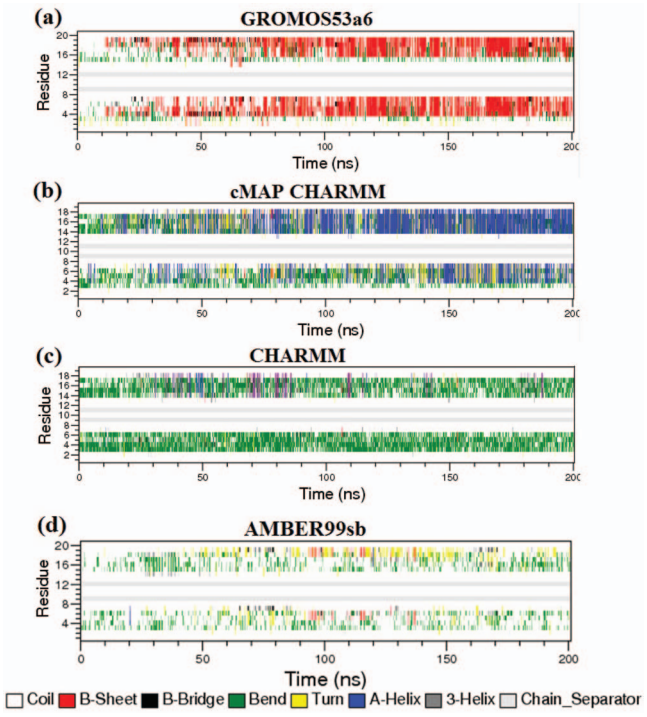

FIG. 3. Evolution of secondary structure of B2088 in water at 298 K from the REMD simulations.

The delicate balance between intramolecular interactions and solvation influence the compactness of any polymer. For B2088, we examined this over the last 100 ns of the REMD simulations, through the Rg and the exposed Sa, which are a measure of compactness of a structure[45] (Figures S3, S4, and 4; Table I). The surface area was calculated using a probe with radius 0.14 nm. As expected, the four force fields show totally different free energy landscapes. GROMOS53a6 predicts a single minimum in the free energy surface, corresponding to the β-sheet structure formed between the two branches (as mentioned above) with the most probable values for Rg and Sa being 0.98 nm and 23.8 nm^2, respectively. In comparison, both cMAP CHARMM and CHARMM predict a more

TABLE I. Most probable values of Rg, Sa, Rgc in solution and in the presence of micelles.

	Rg (nm) in water	Sa (nm^2) in water	Rg (nm) in micelle	Sa(nm^2) in micelle	Rgc (nm) in micelle
NMR	NA	NA	0.91	25.9	1.11
GROMOS53a6	0.98	23.8	1.27	29.2	1.64
cMAP CHARMM	0.87	23	1.08	26.5	1.307
CHARMM	0.91	23.3	0.92	23.8	1.127
AMBER99sb	1.03	25.1	1.38	28.5	1.577

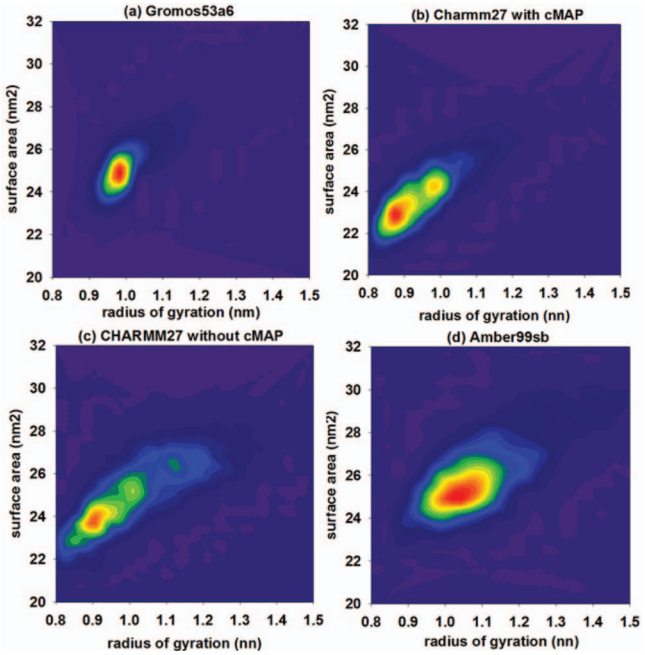

FIG. 4. Free energy landscape of B2088 in water (298 K). The free energy is represented in terms of probability, which is based on the last 100 ns of a 200 ns REMD run.

complex free energy landscape, indicating a flexible structure of B2088. It can be seen in Figure 4(b) that besides the main minimum at Sa = 23.9 nm^2 and Rg = 0.87 nm, there is a secondary minimum at Sa = 24.5 nm^2 and Rg = 0.97 nm in the case of cMAP CHARMM. Removal of the cMAP correction leads to increased flexibility; for example, with cMAP, Rg ranges from 0.85 nm to 1.06 nm and Sa from 21.7 nm^2 to 25.2 nm^2; while in the case of no cMAP correction, B2088 samples a larger region of the phase space, with Rg ranging from 0.85 nm to 1.2 nm and Sa from 22 nm^2 to 26.5 nm^2. The AMBER99sb force field produces a single minimum in the free energy landscape; however, the most probable values of Rg and Sa are much larger (Table I) than in the other force fields, indicating a relatively extended structure. In conclusion, we find that CHARMM and AMBER99sb are most suited to reproduce the structural aspects of B2088 in aqueous environments.

B. Structure of the branched peptide B2088 in the presence of lipid micelles

We next carry out MD simulations of B2088 in the presence of micelles, which have been used to mimic the inner membrane of the bacteria.[57–59] In this study, the micelle is made up of 25% negatively charged POPG lipids and 75% zwitterionic DPC lipids. The CD spectra (Figure 2) of B2088 in the lipid and water environments are very similar with a negative minimum around 197 nm, indicating that the peptide lacks any α-helical or β-sheet structures in both environments. NMR data also suggested a coiled structure without any α-helical or β-sheet motifs, yielding an average Rg and Sa of 0.91 nm and 25.9 nm^2, respectively (Table I).

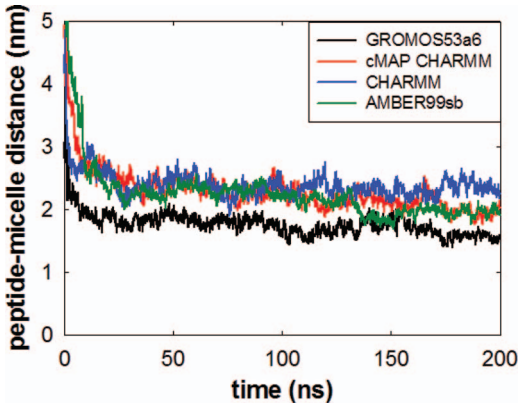

FIG. 5. Peptide-micelle center of mass distance during the simulation.

For the analysis of the simulations of B2088 in the presence of the micelles, we used the distance between the center of mass of B2088 and the center of mass of the micelle to represent the extent of adsorption/penetration of B2088 on/in to the micelle. When placed randomly in solution close (2.5 nm) to the surface of the micelle, the peptide rapidly adsorbed onto the anionic micelle surface (within 20 ns) for all the four force fields studied (Figure 5). This is not surprising and results from the strong electrostatic attraction between the positively charged peptide and the negatively charged micelle. Although the four force fields show similar kinetics of binding, the equilibrium positions of the peptide with respect to the center of mass of the micelle are somewhat different. Three force fields (cMAP CHARMM, CHARMM, and AMBER99sb) show similar peptide-micelle distances of ~2.3 nm. In contrast, the GROMOS53a6 force field predicts a significantly smaller distance (~1.8 nm). The deeper penetration of B2088 into the micelle in the case of GROMOS53a6 suggests that this force field is characterized by more favorable peptide-lipid interactions compared to that encoded within the other three force fields. This is further confirmed by the radial distribution function (RDF) of the atoms of B2088 with respect to the center of mass of the micelle (Figure 6). Again, GROMOS53a6 predicts the closest distance of the first peak of the RDF, followed by CHARMM, cMAP CHARMM, and AMBER99sb. In addition, cMAP CHARMM and AMBER99sb predict a broader peak, indicating weaker

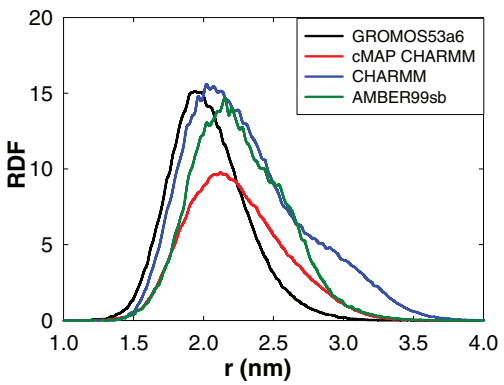

FIG. 6. Radial distribution functions of atoms of B2088 with respect to the center of mass of the micelle.

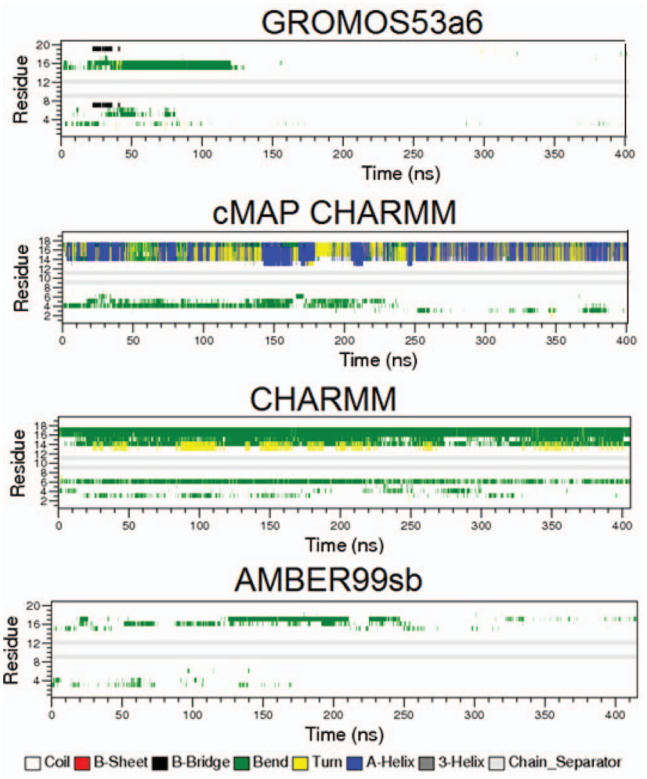

FIG. 7. Secondary structure evolution of B2088 in the presence of DPC-POPG micelle at 298 K.

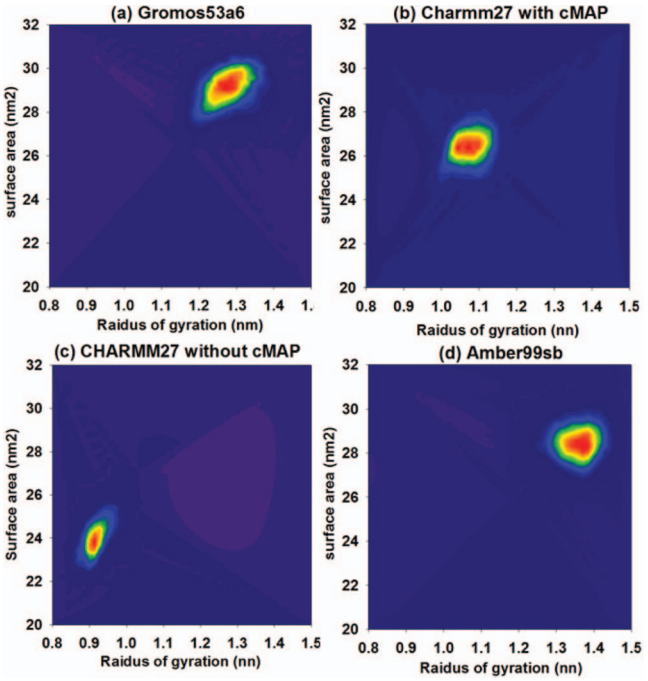

FIG. 8. Free energy landscape of B2088 in the presence of micelle (298 K). The free energy is represented in terms of probability, which is based on the last 200 ns of a 400 ns MD run.

interactions of B2088 with the micelle. Figures 5 and 6 also suggest that B2088 prefers to stay in close proximity to the head groups of the lipids instead of penetrating into the hydrophobic core of the micelle. This is reasonable because B2088 contains only four Val residues in contrast to the majority of its other residues being basic Lys and Arg. The low hydrophobicity will incur a large free energy penalty of transfer from the bulk water to the hydrophobic core of the micelle.

The evolutions of the secondary structure of B2088 in the presence of a micelle (Figure 7) show differences in the topologies of the peptides compared to those in water. The biggest change is seen in the GROMOS53a6 force field, which shows a change from a stable β-sheet structure in water to a coiled structure in the presence of a micelle. Again in cMAP CHARMM, the α-helical structure present in water is largely lost in the presence of micelle. The radius of gyration and surface area of B2088 in the presence of micelle[45] (Figures S5 and S6 of the supplementary material) were calculated and the corresponding free energy landscapes are shown in Figure 8. The differences in the conformations of the peptides between the micelle and the water environments are evident. For all force fields examined in this study, the location of the primary minimum in the free energy landscape shifts to larger Rg and Sa values in the presence of micelle, indicating a less compact structure of B2088. In addition, CHARMM, cMAP CHARMM, and AMBER99sb predict less structural diversity when interacting with the micelle, as can be seen by the smaller region sampled in the free energy landscapes. In particular, the cMAP CHARMM and CHARMM force fields also predict a less complex free energy landscape in the presence of a micelle—there is only a single minimum; in contrast, in water, there is a secondary minimum. However, in the case of GROMOS53a6 and AMBER99sb, B2088 assumes extended structures as can be seen from the shift in Rg and Sa to larger values. Thus, based on the most probable Rg and Sa values in the free energy landscape, the predicted compactness of B2088 in the presence of a micelle using different force fields is: CHARMM < cMAP CHARMM < GROMOS53a6 < AMBER99sb.

Although the distribution of structural parameters (e.g., Rg and Sa) becomes narrow when B2088 binds to the DPC/POPG micelle, its structure remains dynamic, as can be seen from Figure 9 where it is clear that even the NMR structures represent a dynamic ensemble. To examine in detail the differences in the four force fields with respect to the NMR ensemble, we computed the distribution of the pair-wise root mean square deviation (RMSD) between each structure of the NMR ensemble and each structure of the simulated ensembles (Figure 10).[60] The results demonstrate that the ensemble generated using CHARMM is structurally the closest to the NMR ensemble followed by the ensembles generated using cMAP CHARMM. It is clear that the ensembles generated using GROMOS53a6 and AMBER99sb show significantly larger deviations from the NMR generated ensemble.

The dynamical nature of B2088 in water and in the micelles can also be gauged from the autocorrelation functions of the radius of gyration and surface area of the system[45] (Figure S7 of the supplementary material).[45] The rapid decay in the presence of water compared to the slow and semi-periodic nature of the decays in the presence of micelle reflects the fact that the peptides are less dynamic in the presence of micelle and hence undergo more complex dynamics. Similar behavior can be gauged from the autocorrelations of

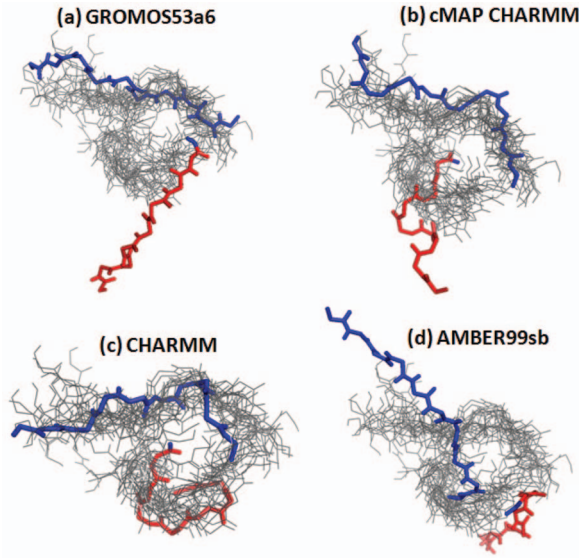

FIG. 9. Comparison of predicted B2088 conformations with the NMR experimental results using structural alignment. The backbones of 20 models of B2088 NMR structure are shown in gray lines, and the backbones of the primary chain (blue) and the secondary chain (red) of B2088 from different force fields are shown in sticks.

the backbone NH bond vector fluctuations (Figure S8 of the supplementary material). In an aqueous environment, the peptides are highly dynamic, while on the surface of the micelle they remain semi-extended with hydrogen bonds between the basic residues and the phosphate groups. The mechanisms that govern this behavior will emerge from groups solvated by water, groups bridged to phosphate groups with water, and groups completely solvated by phosphate groups. This will be accompanied with a slow interchange between the conformations which will result in the complex and slow decay of the autocorrelation functions seen yielding different ruggedness of the landscapes (Figures 4 and 8). Indeed, the exposed surface areas of the sidechain polar groups of Arg and Lys residues[45] (supplementary material Tables S1 and S2) undergo a marked and yet not total reduction in the transition from aqueous to the micelle environment. It is clear that some side chains are deeply buried into the phosphate moieties

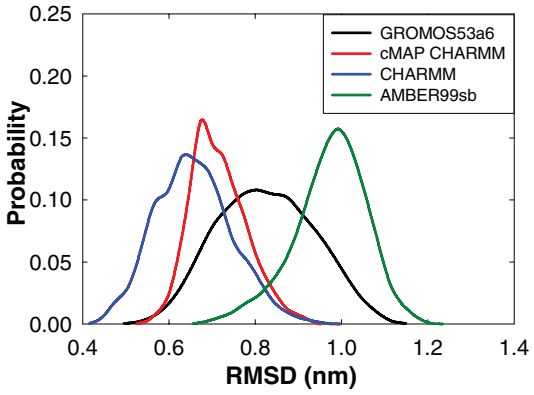

FIG. 10. Distribution of the pair-wise root mean square deviation (RMSD) between structures in the simulated ensembles and structures in NMR ensembles.

while some are partially exposed. The restriction in mobility is also seen in the variance from the most probable structures (Figure S9 of the supplementary material) being large in water and fairly reduced in micelle. Interestingly, other antimicrobial peptides such as magainin was also demonstrated to be quite dynamic in water while relatively stable in membrane-mimicking environment.[61]

The computed Nuclear Overhauser effect (NOE) violations[62,63] shown in Figure S10[45] demonstrate that while the small and highly flexible nature of the peptide underlies the inability of any of the four force fields to capture completely the solution dynamics revealed by NMR, nevertheless the CHARMM force field showed the least number of violations. However, we do note that the literature reporting good agreement between experimental data and simulations has focused on peptides with ordered secondary/tertiary structures.[62,64,65] In addition, it is not yet clear the extent to which NOE violations can be used as a metric for assessing simulations as a recent study has demonstrated that simulations of both non-native and native structures of a protein yield data that match the experimental NOEs of native structures very well.[66] Therefore, we decided to compare the structural data derived from the simulations with that from NMR. We cluster[67] the conformations generated in the case of each force field, and the three most probable structures are aligned together in Figure S11, showing a relatively stable structure of B2088 than that in water. Then the most probable structure of B2088 was aligned with the NMR structure. The NMR structure of B2088 in the presence of micelle is quite dynamic (Figure 9), especially at the N-terminal ends of the two chains. Although the predicted conformations of the primary chain using the four force fields in general agree well with NMR results, GROMOS53a6 and AMBER99sb force fields show large deviations in the conformations of the secondary chain. For example, both GROMOS53a6 and AMBER99sb predict extended conformations of the secondary chain, while NMR suggests coiled conformations. These may arise from overestimations of peptide-lipid interactions and visual inspection shows that B2088 extends along the micelle surface, making several interactions (Figure S12).[45] The cMAP correction leads to larger deviations from the NMR structure, probably due to the overestimation of the helical structure, but it is CHARMM without cMAP correction which yields the closest match between the simulated structure and the NMR structure (Figures 9(b) and 9(c)).

To gain a better understanding of the interaction of B2088 with lipid molecules, we calculated the number of hydrogen bonds between them (Table II). It can be seen that the number of hydrogen bonds using the four force fields are qualitatively similar, but quantitatively different. For example, all the force fields show negligible intra-molecular hydrogen bonds within B2088. In contrast, the majority of hydrogen bonds are formed between peptide and lipid molecules. Unsurprisingly, it is the PO_4 group of lipid molecules that are responsible for the formation of hydrogen bonds with B2088. Further analysis show that the PO_4 group prefers to be hydrogen bonded with the side chains of basic residues Arg and Lys. The high content of these basic residues in B2088 accounts

TABLE II. Number of hydrogen bonds formed between the peptide and micelle. Abbreviations: pep for peptide, side for sidechain of the peptide, back for backbone of the peptide, PO_4 for the phosphate groups of lipids, Gua for the guanidine group of the Arg side chain, and NH_3 for the terminal groups of the Lys side chain. Numbers in bracket represent the standard deviation.

	AMBER99sb	cMAP CHARMM	CHARMM	GROMOS53a6
Pep-pep	2.34 (1.50)	4.69 (1.26)	6.21 (1.17)	2.07 (1.29)
Side-back	2.22 (1.49)	3.38 (1.00)	4.52 (0.72)	0.71 (0.83)
Back-back	0.12 (0.35)	1.31 (0.87)	1.68 (0.94)	1.36 (1.09)
Lipid-pep	30.33 (3.83)	22.35 (4.01)	17.79 (3.11)	37.62 (5.09)
Lipid-side	23.97 (3.26)	17.72 (3.56)	12.21 (2.82)	25.90 (5.83)
Lipid-back	6.36 (1.95)	4.64 (1.48)	5.58 (1.72)	11.72 (1.84)
PO_4-pep	27.46 (3.60)	21.20 (3.70)	15.99 (2.90)	33.26 (5.14)
PO_4-side	23.34 (3.18)	17.10 (3.48)	11.39 (2.77)	24.95 (5.81)
PO_4-back	4.12 (1.70)	4.10 (1.24)	4.59 (1.38)	8.31 (1.38)
PO_4-Gua	22.43 (3.05)	15.35 (3.21)	8.78 (2.28)	16.91 (5.65)
PO_4-NH_3	1.68 (1.10)	2.78 (1.27)	3.61 (1.59)	12.84 (1.05)

for its favorable interactions with lipid molecules. This is consistent with chemical shift data and NOEs from NOESY data in our earlier experiments.[7] Further comparison of the hydrogen bonding ability of the side chains of Arg and Lys suggests that the guanidium group of Arg has a higher ability to form hydrogen bonds with PO_4 groups This arises from the ability of the Arg sidechain to form bidentate hydrogen bonds with the PO_4 groups (Figure S13),[45] consistent with other simulation and experimental studies.[68,69] This, together with observations that the bidentate hydrogen bonds between Arg side chains and PO_4 group of lipids can induce a much larger curvature of the bilayer,[70] suggesting new avenues for the design of novel features into membrane targeted antimicrobial peptides.

Finally, the charge density of B2088 has been shown to be an important parameter determining the antimicrobial activity of B2088.[71] The radius of gyration of the charged groups (Rgc) of B2088 (Figure 11) shows excellent agreement between the CHARMM force field and the NMR derived data, with the other three force fields yielding much larger values.

C. Discussion

We have demonstrated, using atomistic computer simulations, that the small and highly effective novel antibiotic, the branched chain 18-residue cationic peptide B2088, is highly dynamic in conformational space and thus lack a stable structure in water but forms stable conformations in the lipid environment. Several factors affect the conformation of B2088 in water, namely, the branched topology, repulsion between the charged residues, the backbone dihedral potentials, and the peptide-water solvation energies. We study the ability of four commonly used force fields to reproduce the structural dynamics of this peptide as elicited from experimental observations. Among these force fields, GROMOS53a6 predicts a stable structure (β-sheet) of B2088 in water, while all the other force fields predict relatively flexible structures. Although GROMOS53a6 has been shown to overestimate the β-sheet structure in a number of studies, it is still surprising that the highly charged peptide B2088 forms β-sheet structure because of the strong electrostatic repulsion between its charged residues. Several reasons may contribute to the formation of the β-sheet structure. First, the β-sheet structure may result from the cross-linking of the two chains that brings the two branches spatially close enough. In contrast, the effect of branched topology seems to be minor for the other force fields. Another reason may be due to the hydrophobic association between the four Val residues, which was confirmed by visual inspection of the trajectory. The overpopulation of the β-sheet structure using GROMOS53a6 may also occur because of the employment of PME combined with the SPC water models originally developed using cutoff.[23] In the presence of lipid micelles, GROMOS53a6 predicts a more extended structure than in water. The micelle induced conformational changes of B2088 result from strong electrostatic interactions between the positively charged B2088 and the negatively charged lipids. The AMBER99sb force field also fails to reproduce the NMR structure of B2088 in the presence of micelle, although it predicts a coiled structure of B2088 in water, consistent with the CD experiments. Similar to the GROMOS53a6 force field, AMBER99sb yields an extended structure of B2088 in the presence of micelle, in contrast to the compact structure shown in NMR.

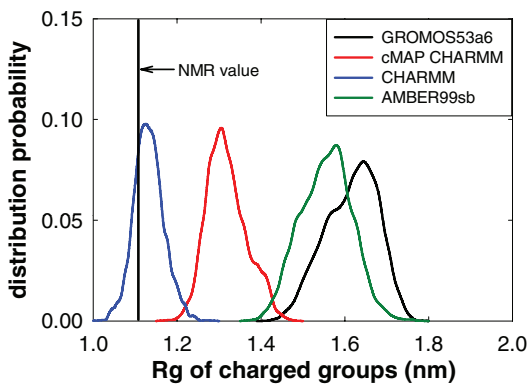

FIG. 11. Radius of gyration based on the charged points of Arg and Lys side chains.

cMAP CHARMM27 overestimates the α-helical structure, which decreases in the presence of micelle. The predicted helical structure is inconsistent with both CD and NMR experiments. Removal of the cMAP correction yields the most compact structure of B2088 both in water and in the presence of micelle, as can be seen from the overall radius of gyration, the surface area and the radius of gyration of the charged groups. Among the four force fields examined in this study, the structure predicted by CHARMM is most consistent with both CD and NMR experiments, as judged by Rg, Sa, RMSD, and Rgc parameters and by structural alignment of the conformations, in both water and in the presence of micelle. The lack of any helical or sheet structure of the peptide B2088 reveals that the secondary structure (either α-helical or β-sheet) of a peptide is not a prerequisite for its antimicrobial activity, although most AMPs have either α-helical or β-sheet structures. In addition, the flexibility of the peptide also seems to be important for its antimicrobial activity; for example, the α-helical antimicrobial peptide magainin-2, has been shown to unfold to a flexible state when inducing membrane pores.[72] This may be linked with its ability to form multiple

interactions with the membrane through its rapidly interconverting conformations.

Despite the force field dependence seen in this study, the simulations shed light on the possible mechanism of action of B2088. In all the force fields examined, B2088 quickly adsorbs on to the micelle surface, resulting from long-range electrostatic interactions between the cationic B2088 and the anionic lipids. Once adsorbed on the micelle surface, the short-range hydrogen bonding interactions of the side chains of Arg and Lys residues with the phosphate head groups of lipid molecules further enhance the binding of the peptide with the micelle. In the case of the bacterial membrane, this may lead to high concentrations of B2088 on the surface of the bacterial membrane.[73] As a result, a large imbalance of mass and charges across the membrane is created, which could lead to membrane depolarization and increased membrane permeability or membrane disruption. In addition, all the four force fields predict that B2088 localizes in the vicinity of the head groups of the lipids, reflecting a preference to remain at the membrane-water interface rather than penetrate into the hydrophobic region of the membrane. This is probably because B2088 contains a large number of charged residues and few hydrophobic residues (only four Val residues), and hence would incur a high free energy barrier for translocation across the membrane. Therefore, our studies suggest that B2088 is unlikely to induce pores and probably surrounds the membrane, as outlined for the carpet mechanism;[74] further studies are in progress to investigate these.

IV. CONCLUSIONS

In this work, we have compared the accuracy of four force fields AMBER99sb, CHARMM, cMAP CHARMM, and GROMOS53a6 in describing the conformational dynamics of a novel cationic antimicrobial peptide B2088 in aqueous and lipid environments. GROMOS53a6 was found to overestimate the β-sheet conformation, while cMAP correction of CHARMM force field overestimates the α-helical conformation. Among the four force fields, CHARMM without cMAP correction was found to most successfully capture the conformational dynamics of B2088 and reproduce trends as elicited from CD and NMR experiments. All four force fields predict favorable interactions of B2088 with the head groups of lipid molecules, indicating a carpeting mechanism of action.

ACKNOWLEDGMENTS

We thank grant support from NMRC/TCR/002-SERI/2008/R618 and ETPL/10-S10FSH-008, Singapore. The authors also thank A*STAR Computational Resource Center for providing the computational facilities.

[1]E. Matyus, C. Kandt, and D. P. Tieleman, Curr. Med. Chem. **14**(26), 2789–2798 (2007).
[2]A. Izadpanah and R. L. Gallo, J. Am. Acad. Dermatol. **52**(3), 381–390 (2005).
[3]M. R. Yeaman and N. Y. Yount, Pharmacol. Rev. **55**(1), 27–55 (2003).
[4]M. Zasloff, Nature (London) **415**(6870), 389–395 (2002).
[5]T. Ganz, Nat. Rev. Immun. **3**(9), 710–720 (2003).
[6]S. Liu, L. Zhou, R. Lakshminarayanan, and R. Beuerman, Int. J. Pept. Res. Ther. **16**(3), 199–213 (2010).
[7]Y. Bai, S. Liu, J. Li, R. Lakshminarayanan, P. Sarawathi, C. Tang, D. Ho, C. Verma, R. W. Beuerman, and K. Pervushin, J. Biol. Chem. **287**(32), 26606–26617 (2012).
[8]L. Zhou, S. P. Liu, L. Y. Chen, J. Li, L. B. Ong, L. Guo, T. Wohland, C. C. Tang, R. Lakshminarayanan, J. Mavinahalli, C. Verma, and R. W. Beuerman, Amino Acids **40**(1), 123–133 (2011).
[9]Y. He, L. Prieto, and T. Lazaridis, Biophys. J. **100**(3, Suppl. 1), 497a (2011).
[10]K. Hall, T.-H. Lee, and M.-I. Aguilar, J. Mol. Recognit. **24**(1), 108–118 (2011).
[11]D. J. Schibli, H. N. Hunter, V. Aseyev, T. D. Starner, J. M. Wiencek, P. B. McCray, B. F. Tack, and H. J. Vogel, J. Biol. Chem. **277**(10), 8279–8289 (2002).
[12]L. D. Schuler, X. Daura, and W. F. van Gunsteren, J. Comput. Chem. **22**(11), 1205–1218 (2001).
[13]A. D. Mackerell, M. Feig, and C. L. Brooks, J. Comput. Chem. **25**(11), 1400–1415 (2004).
[14]W. D. Cornell, P. Cieplak, C. I. Bayly, I. R. Gould, K. M. Merz, D. M. Ferguson, D. C. Spellmeyer, T. Fox, J. W. Caldwell, and P. A. Kollman, J. Am. Chem. Soc. **117**(19), 5179–5197 (1995).
[15]W. L. Jorgensen and J. Tirado-Rives, J. Am. Chem. Soc. **110**(6), 1657–1666 (1988).
[16]V. Hornak, R. Abel, A. Okur, B. Strockbine, A. Roitberg, and C. Simmerling, Proteins: Struc., Funct., Bioinf. **65**(3), 712–725 (2006).
[17]A. E. García and K. Y. Sanbonmatsu, Proc. Natl. Acad. Sci. U.S.A. **99**(5), 2782–2787 (2002).
[18]Y. Duan, C. Wu, S. Chowdhury, M. C. Lee, G. Xiong, W. Zhang, R. Yang, P. Cieplak, R. Luo, T. Lee, J. Caldwell, J. Wang, and P. Kollman, J. Comput. Chem. **24**(16), 1999–2012 (2003).
[19]D. J. Price and C. L. Brooks, J. Comput. Chem. **23**(11), 1045–1057 (2002).
[20]A. Lakdawala, M. Wang, N. Nevins, D. Liotta, D. Rusinska-Roszak, M. Lozynski, and J. Snyder, BMC Chem. Biol. **1**(1), 2 (2001).
[21]F. Bresme, E. Chacón, and P. Tarazona, Mol. Phys. **108**(14), 1887–1898 (2010).
[22]T. Yoda, Y. Sugita, and Y. Okamoto, Chem. Phys. **307**(2–3), 269–283 (2004).
[23]D. Matthes and B. L. de Groot, Biophys. J. **97**(2), 599–608 (2009).
[24]O. F. Lange, D. van der Spoel, and B. L. de Groot, Biophys. J. **99**(2), 647–655 (2010).
[25]S. Kawamoto, M. Takasu, T. Miyakawa, R. Morikawa, T. Oda, S. Futaki, and H. Nagao, J. Chem. Phys. **134**(9), 095103 (2011).
[26]W. A. Hegefeld, S.-E. Chen, K. Y. DeLeon, K. Kuczera, and G. S. Jas, J. Phys. Chem. A **114**(47), 12391–12402 (2010).
[27]S. Gnanakaran and A. E. García, Proteins: Struct., Funct., Bioinf. **59**(4), 773–782 (2005).
[28]Z. Shi, C. A. Olson, G. D. Rose, R. L. Baldwin, and N. R. Kallenbach, Proc. Natl. Acad. Sci. U.S.A. **99**(14), 9190–9195 (2002).
[29]J. Graf, P. H. Nguyen, G. Stock, and H. Schwalbe, J. Am. Chem. Soc. **129**(5), 1179–1189 (2007).
[30]R. B. Best, N.-V. Buchete, and G. Hummer, Biophys. J. **95**(1), L07–L09 (2008).
[31]T. Yoda, Y. Sugita, and Y. Okamoto, Chem. Phys. Lett. **386**(4–6), 460–467 (2004).
[32]D. van der Spoel and M. M. Seibert, Phys. Rev. Lett. **96**(23), 238102 (2006).
[33]N. V. Buchete and G. Hummer, Phys. Rev. E **77**(3), 030902 (2008).
[34]C. Oostenbrink, A. Villa, A. E. Mark, and W. F. Van Gunsteren, J. Comput. Chem. **25**(13), 1656–1676 (2004).
[35]A. D. MacKerell, N. Banavali, and N. Foloppe, Biopolymers **56**(4), 257–265 (2000).
[36]S. A. Showalter and R. Bruschweiler, J. Chem. Theory Comput. **3**(3), 961–975 (2007).
[37]A. E. Aliev and D. Courtier-Murias, J. Phys. Chem. B **114**(38), 12358–12375 (2010).
[38]L. Wickstrom, A. Okur, and C. Simmerling, Biophys. J. **97**(3), 853–856 (2009).
[39]L. Rosso and I. R. Gould, J. Comput. Chem. **29**(1), 24–37 (2008).
[40]S. W. I. Siu, R. Vacha, P. Jungwirth, and R. A. Bockmann, J. Chem. Phys. **128**(12), 125103 (2008).
[41]P. Bjelkmar, P. Larsson, M. A. Cuendet, B. Hess, and E. Lindahl, J. Chem. Theory Comput. **6**(2), 459–466 (2010).
[42]W. L. Jorgensen and J. D. Madura, J. Am. Chem. Soc. **105**(6), 1407–1413 (1983).

[43]H. J. C. Berendsen, J. P. M. Postma, W. F. van Gunsteren, and J. Hermans, in *Intermolecular Forces*, edited by B. Pullmann (Reidel, Dordrecht, 1981), p. 331.
[44]A. Patriksson and D. van der Spoel, Phys. Chem. Chem. Phys. **10**(15), 2073–2077 (2008).
[45]See supplementary material at http://dx.doi.org/10.1063/1.4768899 for Figures S1–S13 and Tables S1 and S2.
[46]W. Kabsch and C. Sander, Biopolymers **22**(12), 2577–2637 (1983).
[47]H. J. C. Berendsen, J. P. M. Postma, W. F. Vangunsteren, A. Dinola, and J. R. Haak, J. Chem. Phys. **81**(8), 3684–3690 (1984).
[48]O. Berger, O. Edholm, and F. Jähnig, Biophys. J. **72**(5), 2002–2013 (1997).
[49]J. B. Klauda, R. M. Venable, J. A. Freites, J. W. O'Connor, D. J. Tobias, C. Mondragon-Ramirez, I. Vorobyov, A. D. MacKerell, and R. W. Pastor, J. Phys. Chem. B **114**(23), 7830–7843 (2010).
[50]J. Wang, W. Wang, P. A. Kollman, and D. A. Case, J. Mol. Graphics Modell. **25**(2), 247–260 (2006).
[51]J. Wang, R. M. Wolf, J. W. Caldwell, P. A. Kollman, and D. A. Case, J. Comput. Chem. **25**(9), 1157–1174 (2004).
[52]P. Güntert, Methods Mol. Biol. **278**, 26 (2004).
[53]M. Buck, S. Bouguet-Bonnet, R. W. Pastor, and A. D. MacKerell, Biophys. J. **90**(4), L36–L38 (2006).
[54]M. Feig, A. D. MacKerell, and C. L. Brooks, J. Phys. Chem. B **107**(12), 2831–2836 (2003).
[55]P. L. Freddolino, S. Park, B. Roux, and K. Schulten, Biophys. J. **96**(9), 3772–3780 (2009).
[56]C. Löw, U. Weininger, H. Lee, K. Schweimer, I. Neundorf, A. G. Beck-Sickinger, R. W. Pastor, and J. Balbach, Biophys. J. **95**(9), 4315–4323 (2008).
[57]H. Khandelia and Y. N. Kaznessis, Peptides **27**(6), 1192–1200 (2006).
[58]A. A. Langham, H. Khandelia, and Y. N. Kaznessis, Peptide Sci. **84**(2), 219–231 (2006).
[59]S. Bourbigot, E. Dodd, C. Horwood, N. Cumby, L. Fardy, W. H. Welch, Z. Ramjan, S. Sharma, A. J. Waring, M. R. Yeaman, and V. Booth, Biopolymers **91**(1), 1–13 (2009).
[60]S. Lukman, D. Wales, and C. S. Verma, Proteins: Struct., Funct., Bioinf. **80**(4), 1066–1077 (2012).
[61]F. Mehrnejad, M. M. Ghahremanpour, M. Khadem-Maaref, and F. Doustdar, J. Chem. Phys. **134**(3), 035104 (2011).
[62]B. Zagrovic, Z. Gattin, J. Lau, M. Huber, and W. van Gunsteren, Eur. Biophys. J. **37**(6), 903–912 (2008).
[63]Z. Gattin, J. Zaugg, and W. F. van Gunsteren, ChemPhysChem **11**(4), 830–835 (2010).
[64]R. Bürgi, X. Daura, A. Mark, W. Van Gunsteren, M. Bellanda, S. Mammi, and E. Peggion, J. Pept. Res. **57**(2), 107–118 (2001).
[65]N. Schmid, J. Allison, J. Dolenc, A. Eichenberger, A.-P. Kunz, and W. van Gunsteren, J. Biomol. NMR **51**(3), 265–281 (2011).
[66]B. Zagrovic and W. F. van Gunsteren, Proteins: Struct., Funct., Bioinf. **63**(1), 210–218 (2006).
[67]X. Daura, K. Gademann, B. Jaun, D. Seebach, W. F. van Gunsteren, and A. E. Mark, Angew. Chem., Int. Ed. **38**(1–2), 236–240 (1999).
[68]Y. Su, A. J. Waring, P. Ruchala, and M. Hong, Biochemistry **49**(29), 6009–6020 (2010).
[69]J. G. Li, M. Garg, D. Shah, and R. Rajagopalan, J. Chem. Phys. **133**(5), 054902 (2010).
[70]N. Schmidt, A. Mishra, G. H. Lai, and G. C. L. Wong, FEBS Lett. **584**(9), 1806–1813 (2010).
[71]Y. Bai, S. P. Liu, P. Jiang, L. Zhou, J. Li, C. Tang, C. Verma, Y. G. Mu, R. W. Beuerman, and K. Pervushin, Biochemistry **48**(30), 7229–7239 (2009).
[72]H. Leontiadou, A. E. Mark, and S. J. Marrink, J. Am. Chem. Soc. **128**(37), 12156–12161 (2006).
[73]W. C. Wimley, ACS Chem. Biol. **5**(10), 905–917 (2010).
[74]Y. Shai and Z. Oren, Peptides **22**(10), 1629–1641 (2001).